Published in final edited form as:

Proc SPIE Int Soc Opt Eng. 2013 March 6; 8668: 866806–. doi:10.1117/12.2006430.

Design considerations for a new, high resolution Micro-Angiographic Fluoroscope based on a CMOS sensor (MAF-CMOS)

Brendan Loughran[*], **S. N. Swetadri Vasan**, **Vivek Singh**, **Ciprian N. Ionita**, **Amit Jain**, **Daniel R. Bednarek**, **Albert Titus**, and **Stephen Rudin**

Toshiba Stroke and Vascular Research Center, University at Buffalo, Buffalo, NY 14214

Abstract

The detectors that are used for endovascular image-guided interventions (EIGI), particularly for neurovascular interventions, do not provide clinicians with adequate visualization to ensure the best possible treatment outcomes. Developing an improved x-ray imaging detector requires the determination of estimated clinical x-ray entrance exposures to the detector. The range of exposures to the detector in clinical studies was found for the three modes of operation: fluoroscopic mode, high frame-rate digital angiographic mode (HD fluoroscopic mode), and DSA mode. Using these estimated detector exposure ranges and available CMOS detector technical specifications, design requirements were developed to pursue a quantum limited, high resolution, dynamic x-ray detector based on a CMOS sensor with 50 μm pixel size. For the proposed MAF-CMOS, the estimated charge collected within the full exposure range was found to be within the estimated full well capacity of the pixels. Expected instrumentation noise for the proposed detector was estimated to be 50–1,300 electrons. Adding a gain stage such as a light image intensifier would minimize the effect of the estimated instrumentation noise on total image noise but may not be necessary to ensure quantum limited detector operation at low exposure levels. A recursive temporal filter may decrease the effective total noise by 2 to 3 times, allowing for the improved signal to noise ratios at the lowest estimated exposures despite consequent loss in temporal resolution. This work can serve as a guide for further development of dynamic x-ray imaging prototypes or improvements for existing dynamic x-ray imaging systems.

Keywords

MAF; CMOS; ROI; fluoroscopy; angiography; x-ray imaging; detector design; neurovascular interventions

1. INTRODUCTION

Our group has previously reported on the high-resolution, dynamic Micro-Angiographic Fluoroscope (Figure 1) based on a CCD sensor (MAF-CCD).[1,2] Despite recently reported clinical success[2–4], there are issues which if resolved would improve the overall

[*]bmloughr@buffalo.edu, Phone: (716) 829-5390, Fax: (716) 854-1850.

effectiveness of the MAF-CCD. In particular, the long length of the detector, when properly deployed in front of the flat panel display (FPD) adds bulk in the direction of the incoming x-rays and increases the risk of collision between the detector and other objects or personnel in the procedure room (Figure 2). The long length of the detector also means that more space is needed between the FPD and the patient when the detector is deployed. This may take time away from the procedure to properly deploy and position the MAF-CCD. Shortening the detector length would eliminate these issues by reducing collision risk and minimizing the time lost to MAF-CCD deployment and positioning. The detector also requires a light tight optical chain to channel the x-ray scintillations into the CCD camera. The interface between each component of the detector is coupled to its adjacent component using optical coupling gel. However, the coupling is fragile at the interface between the fiber optic taper (FOT) and the fiber optic plate (FOP) leading the CCD due to the interface's small physical area. Incidental bumps and movements can lead to this interface becoming decoupled during the use of the MAF. Increasing the interface's total area would reduce this coupling issue and make coupling more stable.

In order to accomplish these detailed improvements, we are proposing a redesign of the MAF-CCD. The new device will use an array of low noise CMOS chips which until relatively recently were not able to be economically fabricated. The array of chips will cover the same total imaging area as the MAF-CCD making the taper of the optical chain unnecessary. Without the FOT, the length of the detector will be significantly reduced and the coupling issues between the FOT and FOP on CCD will be eliminated. There will also be a measurable improvement in the total MTF of the detector as the FOT contributes to substantial degradation in spatial resolution.

In addition, we will explore the option to eliminate the light image intensifier (LII) from the new MAF design. The MAF-CCD utilized the LII to increase the light signal to the CCD chip, thus improving the exposure signal to noise ratio, and increasing the dynamic range of the detector so that both fluoroscopic and angiographic x-ray exposure ranges could be imaged without saturation and could also remain quantum limited. The LII, although a satisfactory solution to the problems faced with the previous MAF-CCD, contributes to the length of the device in the beam direction, somewhat degrades the image quality at the high spatial frequencies [1], adds to device complexity and expense, and requires another optic coupling interface. If feasible, the elimination of the LII would further address the issues of detector length and coupling.

Two preliminary designs are being considered: a MAF-CMOS with an LII and a MAF-CMOS without an LII. The purpose of this work is to use the clinical data acquired by the MAF-CCD along with reasonable assumptions of the technical characteristics of currently available CMOS image sensors to assess the necessary preliminary design characteristics of the proposed MAF-CMOS (Figure 3 and 4). The necessity of including the LII in the new design of MAF-CMOS will also be evaluated.

2. METHODS AND MATERIALS

2.1 Description and use of the MAF-CCD

The MAF-CCD detector is meant to be a high-resolution, region of interest (ROI) x-ray detector for use during neuro-endovascular image-guided interventions (neuro-EIGIs) and has been proposed for use in other types of endovascular interventions. The current imaging standard, flat panel detectors (FPDs) based on indirect detecting amorphous silicon thin film transistor (TFT) solid state circuits, lack the fine resolution, low noise, and overall image quality necessary to detect the extremely small, detailed structure of devices used commonly in neuro-EIGIs. The MAF has significantly better resolution, signal to noise ratios, and use of dose than FPDs.[1] Because the MAF-CCD has a significantly smaller field-of-view as compared to most FPDs, it is not meant to replace the FPD. In neuro-EIGIs, the large field of view of the FPD would still be needed for guidance of the endovascular devices from the minimally invasive entrance point (typically at the femoral artery) to the site of the stenosed vessel or aneurysm. However, once at the affected portion of the vasculature, the MAF-CCD is used as an “x-ray microscope” at this critical time in the procedure when higher resolution is needed to observe fine blood flow, to discern small devices, and to precisely position and deploy interventional tools. The use of the MAF-CCD in 15 clinical neuro-endovascular cases has been reported thus far.[2–4]

2.2 Identification of clinical exposure levels

Any x-ray detector has a limited useful exposure dynamic range. The lower limit is defined by the instrumentation noise equivalent exposure (INEE).[5] The upper limit is defined by the exposure which saturates the detector image. To identify the desired range of exposures for the proposed MAF-CMOS design, the exposure values that the detector is likely to encounter in clinical situations must be determined. Because the proposed detector will be used in the same clinical situations and is expected to have the same detector area as the MAF-CCD, the previous clinical tests of the MAF-CCD are used as a reference to describe the technique parameters that are expected to be used with the MAF-CMOS.[2–4] Of the fifteen clinical tests, much of the information from certain runs is incomplete. During the use of the MAF-CCD, the necessary technique parameters may not have been recorded, the detector may not have been used at critical times, or the detector prototype may have malfunctioned. Discounting these runs, of the fifteen, six runs with their technique parameters were used to find the estimated exposure due to the detector working as it was designed (Table 1).

The exposure to the MAF-CCD detector is estimated by reproducing previous clinical MAF procedures in the laboratory with an x-ray system of similar design and filtration and a phantom of 21 mm of aluminum to mimic the x-ray attenuation and scatter from a human skull.[6] Because of technique limitations of the laboratory x-ray system, the exposures were measured at multiple mAs settings for multiple kV settings and in both fluoroscopic and radiographic x-ray system modes. Using these exposure values, linear curves were interpolated so that all potential exposures experienced by the MAF-CCD in the clinic could be approximated despite limitations on the output of the x-ray machine present in the laboratory. By this method, the expected exposure ranges to the MAF-CMOS detector for all

proposed modes of operation, fluoroscopic mode, HD fluoroscopic mode (radiographic exposure mode at fluoroscopic speeds of up to 30 frames per second), and DSA mode, are estimated.

2.3 Detection of x-rays, conversion to light and electrons, and calculation of charge collected

From these ranges of exposures, the number of electrons collected per unit of exposure is estimated. The standard RQA5 x-ray spectrum uses a 70 kV x-ray beam through a simulated patient thickness with a 21 mm thick aluminum filter added to the inherent tube filtration which results in a beam with a 6.97 mm of aluminum half value layer.[7] Using a standard RQA5 x-ray spectrum, generated by SpekCalc software,[8] the approximate x-ray photon fluence exiting the simulated patient is calculated using the methods described in chapter one of the Handbook of Medical Imaging.[9] This results in a value of x-ray photons per area per exposure of 276 photons per mm^2 per μR. Using this value, the expected pixel area of the proposed detector, and the interpolated exposure found using the method described above, the total number of x-ray photons incident on each pixel of the proposed detector is estimated. Next, the total number of x-ray photons are used in a zero spatial frequency linear cascade model of each imaging stage to determine the total number of electrons expected to be collected by the electron well of the detector. First, an x-ray scintillator with attenuation dependent upon thickness converts the energy of the interacting x-ray photons to light at a rate of one 560 nm light photon for every 18 eV of energy deposited.[10] Two types of CsI x-ray scintillators are considered. The first scintillator type, High Light (HL) type has a reflective layer to direct all light into the FOP and creates 2175 light photons for each interacting x-ray photon in the 54 keV average energy RQA5 x-ray spectrum and has a reflective layer to direct all the light into the FOP.[1] The second scintillator type, High Light (HR) type, converts the same amount of interacting x-ray photon energy to light but does not have the reflective layer so roughly 40% of the light is lost.[11] Once channeled through a fiber optic plate (FOP), the light is either amplified by the LII, or channeled directly onto the CMOS chip. Assuming a reasonable light loss through the FOP of 60%[1] and a realistic quantum efficiency (40–60%),[12] here chosen to be 45% at the CMOS sensor pixel area, the charge collected per pixel and the resultant quantum noise at the zero spatial frequency of the linear cascade model is realistically approximated. Non-zero frequency response is outside the scope of the present paper.

2.4 Estimation of full well capacity and instrumentation noise

In order for the detector to be quantum limited at the lowest exposures likely to be experienced during neuro-EIGIs, the INEE must be smaller than the exposure equivalent quantum noise experienced at all exposures. Put more simply, the instrumentation noise must be lower than the quantum noise. The fabrication process to be used in the construction of the sensor is assumed to be a standard CMOS process used by other commercially CMOS sensors available for medical imaging. Therefore, the full well capacity and instrumentation noise at each pixel should be relative to the levels associated with similar CMOS imaging sensors when corrected for differences due to area dependent pixel capacitance. The reported full well capacity and noise, which is assumed here to be analogous to

instrumentation noise, of commercially available CMOS chips is presented. These reported values establish a range of likely technical limitations for the proposed MAF-CMOS.

2.5 Effect of temporal filter on effective signal and noise

The MAF-CMOS may also implement a recursive temporal filter on the acquired image series in its software to increase the signal to noise per frame. Typical recursive temporal filters use k-constants of values 0–1 or the inverse of these values 1–∞ represented by ω as shown in the equation below

$$S_N = \sum_{m=0}^{N} k(1-k)^m I_{N-m} = \sum_{m=0}^{N} \frac{(1-1/\omega)^m}{\omega} I_{N-m}. \quad (1)$$

Each image of the series is represented as a matrix (I_{N-m}) of numerical gray levels. The total signal displayed (S_N) is a summation of all the total weighted images. The total number of images is N and m is the index of the particular weighted image. As ω increases, the filter increases the weight given to the earlier image matrices, increasing the effect of added lag and reducing noise on the final image. As a result, when assuming an infinite series of image matrices, the recursive temporal filter[13] reduces the total image noise as the ω-constant increases shown below as

$$\sigma_{eff}^2 = \frac{k^2}{2-k}\sigma_o^2 = \frac{1}{2\omega^2-\omega}\sigma_o^2. \quad (2)$$

It is expected that the MAF-CMOS will use the same temporal filter as used with the MAF-CCD. From experience with the MAF-CCD, the ω-constant used typically ranged from 3–5; however, this noise reduction technique comes at the cost of increased motion blur when movement is present in the image and will only be effective for situations where there is little motion and increased lag is acceptable.

2.6 Determination of the necessity of a light image intensifier

In order for the proposed detector to remain unsaturated at the highest estimated exposure, this exposure must not produce more electrons than can be collected by the electron full well capacity of the pixels of the detector's CMOS sensor. For the detector to be quantum noise limited at a given exposure to the detector, the total number of electrons collected should result in a quantum noise that is greater than the number of electrons in the instrumentation noise. Therefore, for the MAF-CMOS to not require any additional gain or a LII, the quantum noise measured in number of electrons collected by the CMOS sensor at the lowest estimated entrance exposure must be larger than the number of electrons which are expected constitute the instrumentation noise. If the quantum noise is less than the instrumentation noise, it is likely that an LII will be needed to boost the number of light photons incident on the CMOS sensor at the lowest estimated exposure so that the detector is quantum noise limited at all exposure levels.

2.7 Check for adequate contrast at lowest estimated fluoroscopic exposure

With the total dynamic range of the proposed MAF-CMOS found in terms of both exposure and electrons, the detector must ensure that digitization noise does not degrade image quality so that both adequate contrast and negligible digitization noise is provided at the lowest estimated fluoroscopic exposure to the detector. Using the FPD, which again is the current imaging standard for neuro-EIGIs, it can be assumed that when recorded by the FPD at low fluoroscopic exposure levels (~2 μR) to the detector, the digital numbers (DNs) in an image of a uniform patient phantom of 21 mm of aluminum provides adequate image contrast and negligible digitization noise. Using the average image DN recorded by the FPD and neglecting the contribution of instrumentation noise to the DN, this DN value divided by the fluoroscopic exposure will give the fluoroscopic DN/μR. To ensure adequate image contrast and negligible digitization noise, the DN value at the lowest fluoroscopic exposure for the MAF-CMOS should be equal to or greater than this DN value for the FPD, while again neglecting the contribution to the DN of the instrumentation noise. Using the estimated maximum number of electrons that can be collected by the CMOS sensor's electron wells divided by the maximum gray level will give the e-/DN of the detector. Next, dividing the number of electrons collected at the lowest estimated fluoroscopic exposure by the lowest estimated fluoroscopic exposure will determine the e-/μR for the MAF-CMOS. Dividing the e-/μR by the e-/DN of the detector results in the DN/μR of the MAF-CMOS. The DN/μR for the MAF-CMOS can also be calculated by simply dividing the expected maximum gray level value by the maximum estimated exposure to the detector. Finally, multiplying the DN/μR by the lowest estimated fluoroscopic exposure gives the lowest average DN value for the proposed MAF-CMOS which can then be compared to the lowest average DN value for the FPD.

3. RESULTS AND DISCUSSION

A well collimated x-ray beam produced by a Toshiba Infinix x-ray system was attenuated by a uniform head phantom of 21 mm of aluminum. The technique parameter dependent and automatic exposure control independent exposure values were recorded for both fluoroscopic and radiographic modes. These exposure values were plotted as a function of the mAs technique parameter and are independent of acquisition frame rate. A linear regression curve was then applied to interpolate the points and find the formula which describes the exposure as a function of the mAs. This was done for all kilovolt potentials and added system filtrations associated with both fluoroscopic (0.2 mm of Cu) and radiographic x-ray imaging modes (1.8 mm of Al) experienced by the MAF-CDD in the clinical tests. The differing filtrations associated with fluoroscopic and radiographic modes produce different x-ray spectra for each kVp setting and therefore result in different estimated exposures to the detector for each mode. The graphs with the linear regression curves and formulas are shown below (Figures 5 and 6).

The above formulas use the technique parameters implemented in the six clinical cases to estimate the highest and lowest exposure values at the entrance of the detector during the clinical tests. It is assumed that these same exposures will also be the highest and lowest exposure values that will be necessary for proper clinical neurological imaging with the

proposed MAF-CMOS. The estimated exposure values to the entrance of the proposed detector after attenuation by the 21 mm thick aluminum uniform head phantom are reported in Table 2. This table also shows the number of x-ray photons per 50 μm pixel that are expected at each exposure value using the assumed fluence of 276 x-photons per mm^2 per μR. The estimated quantum mottle or quantum noise per pixel is also found using linear cascade modeling at the zero frequency and the results are also presented.

The x-ray photons interact with the CsI scintillator to produce light photons which are then channeled through the FOP onto the CMOS sensor. The intensity of the light produced by the scintillator is a function of number of x-rays interacting with the CsI. The number of interactions between the CsI and the x-ray photons is a function of the scintillator's thickness. Once directed onto the sensor, assuming no use of a LII or other light gain stage, the light photons create electrons in proportion to the intensity of incident light. Therefore, the number of electrons collected by the sensor is a function of the number of x-rays interacting with the CsI. The numbers of electrons collected by the CMOS sensor and the resulting quantum noise from CsI scintillators of differing types are shown in Table 3.

The preferred CsI scintillator for the MAF-CMOS will best preserve the high resolution of the small pixel size. Investigations into the GMTF and GDQE of available scintillators find the 500 μm-HR type CsI scintillator an attractive choice.[14–15] We now compare these electron collection values to the values given for current available CMOS detector specifications. Four different detectors with full well capacity and dark noise specifications were found. Their full well capacities and instrumentation noise values are displayed in Table 4.

Based on the results in Table 3 above, the exposure ranges (from low fluoroscopic to high DSA) will produce a range of electrons to be collected on the CMOS chip of 1,400 – 130,000 using the 500μm-HR CsI scintillator. In order to have the instrumentation noise lower than the quantum noise at the lowest fluoroscopic exposure, the instrumentation noise will need to be no larger than 690 electrons, unadjusted for gain and temporal filtering. Using a recursive temporal filter will effectively decrease the noise per frame based on the temporal weight (ω). The common temporal weights used with the MAF-CCD were 3–5 and would decrease the single frame noise by a factor of 2.24 – 3, respectively. For the lowest estimated exposure, this would decrease the effective quantum noise to a range of 230 effective electrons for ω = 5, and to 310 for a ω = 3. The effective instrumentation noise would also drop by the same factor as a result of temporal filtering. As long as the sensor's actual instrumentation noise of the proposed MAF-CMOS does not exceed the stated quantum noise values, the detector will be quantum limited.

Finally, with the proposed MAF-CMOS having a dynamic range of 1,400 – 130,000 electrons without an LII gain stage, the detector must have an appropriate analog to digital converter so that at the lowest estimated exposures digitization noise will not affect the image quality and image contrast. Commonly, CMOS detectors used for radiographic application have 14 bit pixel depth giving a gray level range of 0–16,383 digital numbers. Dividing the maximum possible number of collected electrons by the maximum recordable digital number gives 130,000 e-/16384 DN = 7.93 e-/DN. Taking the lowest estimation of

the amount of collected electrons and dividing by the estimated exposure at this value gives 1,400 e-/8.3 μR = 168.7 e-/μR. Dividing this value by the electrons collected per digital number yields a sensitivity of (168.7 e-/μR)/(7.93 e-/DN) = 21.3 DN/μR. Now, multiplying the sensitivity by the lowest estimated exposure gives the lowest expected average digital number: (21.3 DN/μR)*(8.3 μR) = 176.5 DN. When compared to the lowest average digital number at the lowest expected fluoroscopic exposure of the laboratory FPD, which from experience is 100 DN, the lowest expected digital number for any pixel of the proposed MAF-CMOS: 176.5 DN is significantly higher. Therefore, the proposed MAF-CMOS should have adequate contrast and negligible digitization noise when compared to existing commercial imaging systems.

4. CONCLUSIONS

It may be possible to create the proposed MAF-CMOS detector, ensure that it is always quantum limited, and constrain its use to within the range provided by the full well capacity without the use of the LII gain stage. However, this is dependent on the instrumentation noise specific to the fabricated CMOS sensor. In addition, performance of the proposed detector is only evaluated at the zero frequency in this report. The instrumentation noise value of the Hamamatsu detector appears problematic and is relatively higher than that of the other referenced detectors. Without specific knowledge of the MAF-CMOS detector's noise, a LII gain stage may still be necessary to boost the signal to noise ratio so that the detector operates in the quantum limited region.

According to the information presented above, it appears that with careful design of pixel size, selection of hardware, and temporal filters, a high-resolution, dynamic x-ray detector for fluoroscopy and angiography based on a CMOS chip such as the proposed MAF-CMOS is a possibility. This work does not consider the limitations imposed on the detector due to the instrumentation noise and quantum noise at non-zero spatial frequencies. Differing conclusions may result from such data. Nevertheless, it is expected that if such a detector could be integrated into the clinical neuro-endovascular suite, patient outcomes could be impacted positively.

Acknowledgments

This study was supported in part by NIH Grants R01-EB008425 and R01-EB002873 and an equipment grant from Toshiba Medical Systems Corp.

References

1. Jain A, Bednarek DR, Ionita CN, Rudin S. A theoretical and experimental evaluation of the microangiographic fluoroscope: A high-resolution region-of-interest x-ray imager. Med Phys. 2011; 38 (7):4112–4126. [PubMed: 21859012]
2. Wang W, Ionita C, Huang Y, Qu B, Panse A, Jain A, Bednarek DR, Rudin S. Region-of-interest micro-angiographic fluoroscope detector used in aneurysm and artery stenosis diagnoses and treatment. Proc SPIE. 2012; 8313:831317-1–9.
3. Binning MJ, Orion D, Yasher P, Webb S, Ionita CN, Jain A, Rudin S, Hopkins LN, Siddiqui AH, Levy EI. Use of the Microangiographic Fluoroscope for Coiling of Intracranial Aneurysms. Neurosurgery. 2011; 69(5):1131–1138. [PubMed: 21694658]

4. Kan P, Yasher P, Ionita CN, Jain A, Rudin S, Levy EI, Siddiqui AH. Endovascular coil embolization of a very small ruptured aneurysm using a novel microangiographic technique: technical note. J NeuroIntervent Surg. 2012:1–4. Published Online. 10.1136/neurintsurg-2011-010154
5. Yadava GK, Kuhls-Gilcrist AT, Rudin S, Patel VK, Hoffmann KR, Bednarek DR. A practical exposure-equivalent metric for instrumentation noise in x-ray imaging systems. Phys Med Biol. 2008; 53(18):5107–5121. [PubMed: 18723932]
6. Ionita CN, Loughran B, Jain A, Vasan SNS, Bednarek DR, Levy E, Siddiqui AH, Snyder KV, Hopkins LN, Rudin S. New head equivalent phantom for task and image performance evaluation representative for neurovascular procedures occurring in the Circle of Willis. Proc SPIE. 2012; 8318:83130Q.
7. International Atomic Energy Agency. Technical Reports Series No 457 - Dosimetry in Diagnostic Radiology: An International Code of Practice. IAEA Publishing; Vienna: 2007. p. 69-75.
8. Poludniowski G, Landry G, DeBlois F, Evans PM, Verhaegan F. SpekCalc: a program to calculate photon spectra from tungsten anode x-ray tubes. Phys Med Biol. 2009; 54(19):N433–8. [PubMed: 19724100]
9. Boone, J. Handbook of Medical Imaging: Volume 1. Physics and Psychophysics. Vol. Chapter 1. SPIE Press; Bellingham: 2000. p. 34-50.
10. Rowlands, JA.; Yorkston, J. Handbook of Medical Imaging: Volume 1. Physics and Psychophysics. Vol. Chapter 4. SPIE Press; Bellingham: 2000. p. 244
11. Hamamatsu Corporation. Online Brochure. Feb. 2005 X-ray Scintillator: ACS, ALS, FOS.
12. Esposito M, Anazagoras T, Fant A, Wells K, Konstantinidis A, Osmond JPF, Evans PM, Speller RD, Allinson NM. DynAMITe: a wafer scale sensor for biomedical applications. JINST. 2011; 6:C12058.
13. Hasegawa, B. The Physics of Medical X-Ray Imaging. Vol. Chapter 11. Medical Physics Publishing; Madison: 1987.
14. Gupta, S. Generalized evaluations for improved high-resolution region-of-interest systems. The State University of New York at Buffalo; Buffalo, NY: 2012.
15. Jain A, Bednarek DR, Rudin S. Micro-Angiographic Fluoroscope Input Phosphor Comparison. 2013 Submitted to Phys. Med. Biol., Phys. Med. Biol., Submitted for publication.
16. Arvanitis CD, Bohndiek SE, Blakesley J, Olivo A, Speller RD. Signal and noise transfer properties of CMOS based active pixel flat panel imagers coupled to structured CsI:TI. Med Phys. 2009; 36(1):116–126. [PubMed: 19235380]
17. Arvanitis CD, Bohndiek SE, Royle G, Liang HX, Clark A, Prydderch M, Turchetta R, Speller RD. Empirical electro-optical and x-ray performance evaluation of CMOS active pixels sensor for low dose, high resolution x-ray medical imaging. Med Phys. 2007; 34(12):4612–4625. [PubMed: 18196789]
18. Hamamatsu Corporation. Online Brochure. 2009. Selection Guide: Flat Panel Detectors.

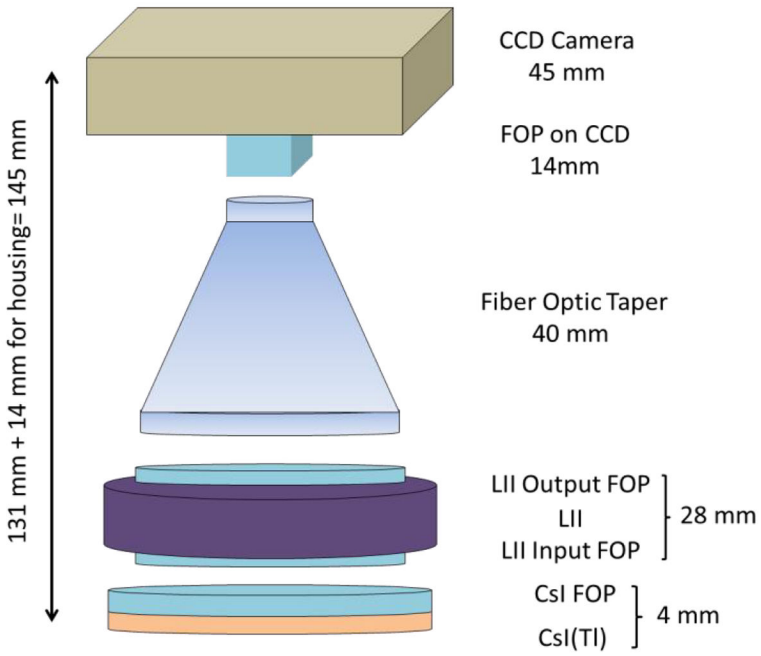

Figure 1.

The internal optical components of the MAF-CCD detector used in clinical tests. The goal is to reduce the overall length of the detector and to improve the stability of coupling between the FOP on CCD and FOT.

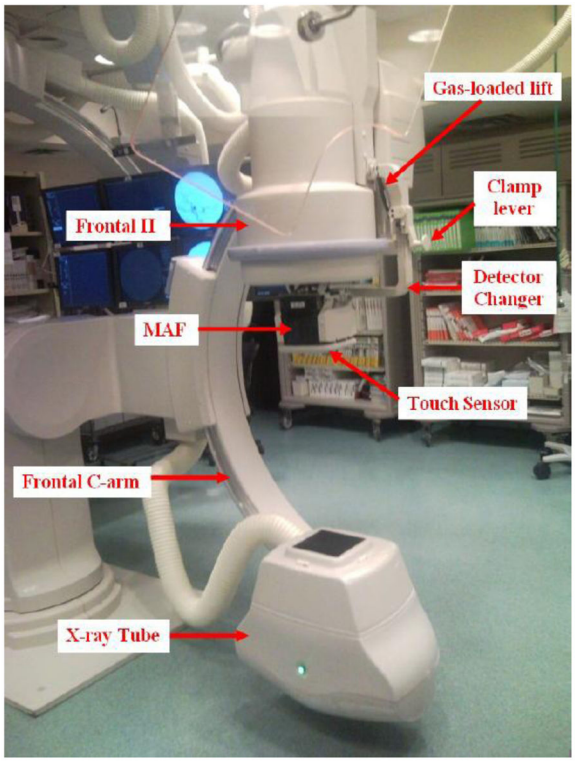

Figure 2.
This figure shows the clinical set up of the MAF-CCD which here is shown in the deployed position. The extra space needed between the patient and FPD can be observed when the MAF-CCD is deployed.

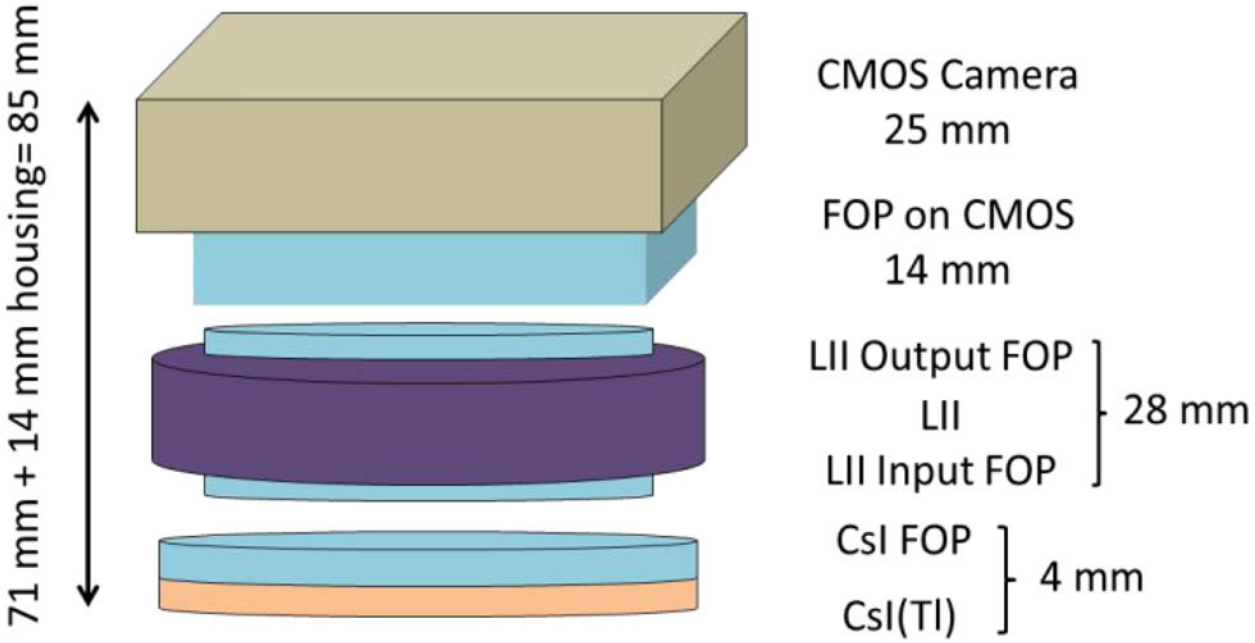

Figure 3.
A schematic of the internal optical components of the proposed MAF-CMOS. The schematic exhibits the expected reduced length from the elimination of the FOT.

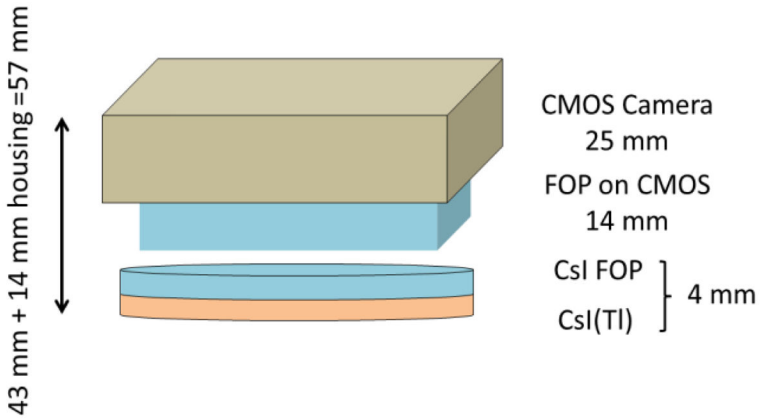

Figure 4.

A schematic of the internal optical components of the proposed MAF-CMOS without the LII. Without the LII the length of the detector is further reduced. This paper also explores the feasibility of this design.

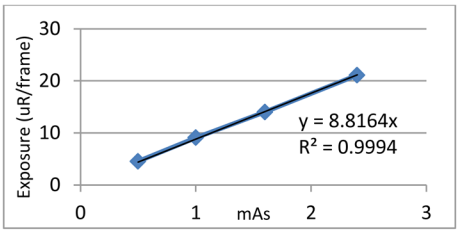

Figure 5a: 80 kV, fluoroscopic mode

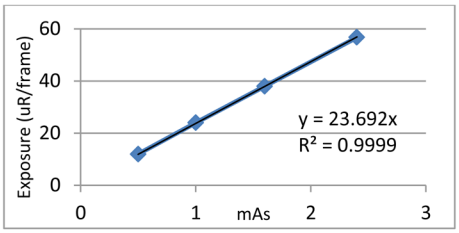

Figure 5c: 90 kV, fluoroscopic mode

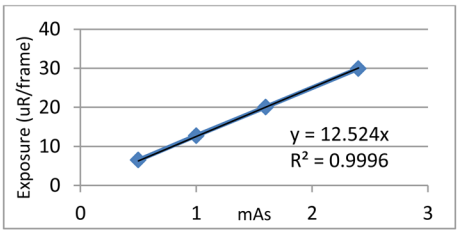

Figure 5b: 86 kV, fluoroscopic mode

Figure 5.

Figures 5a–c: In these graphs, the exposure per frame was found for various machine outputs and various voltage potentials when in fluoroscopic mode. The x-ray system is in fluoroscopic mode only when fluoroscopic imaging mode. The three graphs correspond to the three different voltage potentials used in the six clinical cases. The exposure values were plotted as function of the machine output in mAs. Lines were then interpolated to find a linear formula which correlates the mAs to the exposure input at the detector. The overall maximum and minimum exposures to the detector for the six clinical cases were then calculated using the formulas.

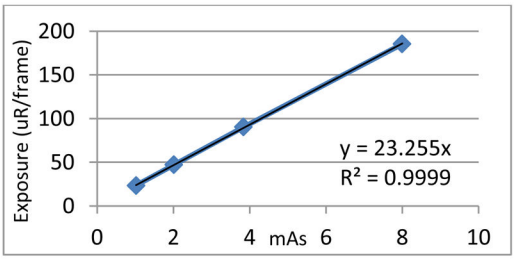

Figure 6a: 80 kV, radiographic mode

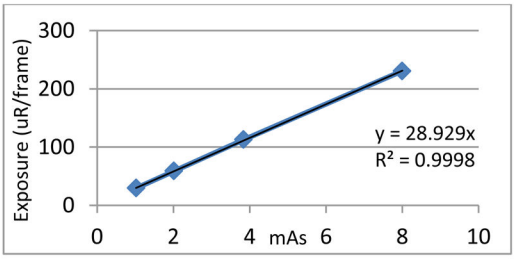

Figure 6b: 84 kV, radiographic mode

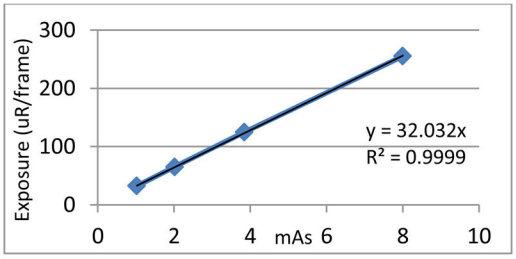

Figure 6c: 86 kV, radiographic mode

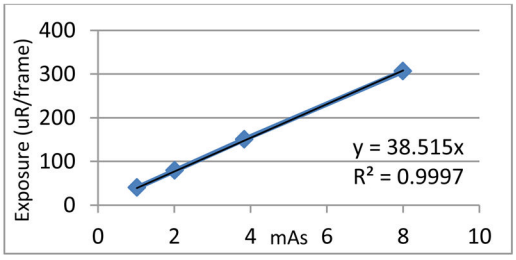

Figure 6d: 90 kV, radiographic mode

Figure 6.

Figures 6a–d: In these graphs, the exposure per frame was found for various machine outputs and various voltage potentials when in radiographic mode. The x-ray system is in radiographic mode for both HD fluoroscopic imaging (30 fps) and DSA imaging mode (3 fps). The four graphs correspond to the four different voltage potentials used in the six clinical cases. The exposure values were plotted as function of the machine output in mAs. Lines were then interpolated to find a linear formula which correlates the mAs to the exposure input at the detector. The overall maximum and minimum exposures to the detector for both HD fluoroscopic and DSA imaging modes for the six clinical cases were then calculated using the formulas.

Table 1

The modes of operation and technique parameters for the six clinical cases used to determine the estimated exposures to the CMOS detector. These cases are explained in more detail elsewhere.[2–4]

	Mode of Operation	Technique Parameters Used			
		kV	mA	ms	mAs
A - Run 2	Fluoro. Mode	90	50	10	0.5
	HD Fluoro.	80	160	20	3.2
	HD Fluoro.	80	160	6.3	1.008
	DSA	86	160	41	6.56
B - Run 4	Fluoro. Mode	90	50	10	0.5
	HD Fluoro.	80	160	20	3.2
C - Run 5	Fluoro. Mode	86	50	13.3	0.665
	DSA	86	160	40	6.4
	DSA	84	160	50	8
	DSA	80	320	50	16
D - Run 7	Fluoro. Mode	90	50	13.3	0.665
	HD Fluoro.	80	160	63	10.08
	DSA	90	250	80	20
E - Run 9	Fluoro. Mode	90	50	10	0.5
	DSA	80	160	25	4
F - Run 14	Fluoro. Mode	90	50	13.3	0.665
	HD Fluoro.	80	160	12	1.92
	HD Fluoro.	80	160	25	4
	DSA	86	160	25	4

Table 2

The exposure per frame range for each mode of detector operation found as described in the methods and materials. The number of x-ray photons per pixel incident on the detector is shown calculated from the number of photons per area per exposure for an RQA5 x-ray spectrum.

--	--	μR/frame	Number of x-ray photons incident to detector per pixel
Fluoroscopy	Low Exp.	8.3	5.7
	High Exp.	15.8	10.9
HD Fluoroscopy	Low Exp.	23.4	16.1
	High Exp.	234.4	161.5
Digital Subtraction Angiography	Low Exp.	93.0	64.1
	High Exp.	770.3	530.6

Table 3

The number of electrons and quantum noise estimated to be collected for CsI scintillators of differing thicknesses and differing types at estimated exposure ranges dictated by the mode of detector operation.

	Electrons collected at fluoroscopic exposures			Electrons collected at HD fluoroscopic (DA) exposures			Electrons collected at DSA exposures		
--	*Low*	*High*	*Noise*	*Low*	*High*	*Noise*	*Low*	*High*	*Noise*
200μm-HR	780	1,480	510–710	2,200	22,000	860–2700	8,750	72,500	1700–4900
200μm-HL	1,370	2,590	900–1200	3,860	38,600	1500–4800	15,300	127,000	3000–8600
300μm-HR	1,050	1,980	590–820	2,940	29,400	1000–3100	11,700	96,700	2000–5700
300μm-HL	1,830	3,460	1000–1400	5,150	51,500	1700–5500	20,400	169,000	3500–10000
350μm-HR	1,150	2,180	620–860	3,250	32,500	1000–3300	12,900	107,000	2100–6000
350μm-HL	2,020	3,820	1100–1500	5,680	56,800	1800–5800	22,500	187,000	3600–10500
500μm-HR	1,400	2,660	690–950	3,950	39,500	1200–3600	15,700	130,000	2300–6600
500μm-HL	2,460	4,650	1200–1700	6,910	69,100	2000–6400	27,400	227,000	4000–11600
600μm-HR	1,520	2,880	720–980	4,290	42,900	1200–3800	17,000	141,000	2400–6900
600μm-HL	2,660	5,040	1300–1700	7,500	75,000	2100–6600	29,800	247,000	4200–12000

Proc SPIE Int Soc Opt Eng. Author manuscript; available in PMC 2013 December 16.

Table 4

The four CMOS detectors used to establish an estimated range of full well capacities and instrumentation noise. Because the full well capacity is a function of the photodiode capacitance and capacitance is a function of area, the full well capacity will differ for different pixel sizes. These full well capacities are taken to be normalized to the pixel area of the proposed MAF-CMOS (50 μm) while the instrumentation noise is taken to be unchanged from the reference detector.

Name of detector	Full Well Capacity (e-)	Pixel Size (μm)	Estimated Full Well Capacity @ 50 μm pixel size	Instrumentation Noise (e-)
Arvenitis (2009)[16]	70,000	25	280,000	50
Arvenitis (2007)[17]	100,000	25	400,000	114
DynAMITe[12]	280,000	50	280,000	150
Hamamatsu[18]	2,200,000	100	550,000	1300